




Perturbed nuclear matter studied within density functional theory with a finite number of particlesF. Marino ^{1,2,*} G. Colò ^{1,2} X. Roca-Maza ^{1,2} and E. Vigezzi²¹*Dipartimento di Fisica “Aldo Pontremoli”, Università degli Studi di Milano, 20133 Milano, Italy*²*INFN, Sezione di Milano, 20133 Milano, Italy*

(Received 15 November 2022; accepted 28 March 2023; published 17 April 2023)

Nuclear matter is studied within the density functional theory framework. Our method employs a finite number of nucleons in a box subject to periodic boundary conditions, in order to simulate infinite matter and study its response to an external static potential. We detail both the theoretical formalism and its computational implementation for pure neutron matter and symmetric nuclear matter with Skyrme-like energy density functionals (EDFs). The implementation of spin-orbit, in particular, is carefully discussed. Our method is applied to the problem of the static response of nuclear matter and the impact of the perturbation on the energies, densities, and level structure of the system is investigated. Our work is a crucial step in our program of *ab initio* based nuclear EDFs [*Phys. Rev. C* **104**, 024315 (2021)] as it paves the way towards the goal of constraining the EDF surface terms on *ab initio* calculations.

DOI: [10.1103/PhysRevC.107.044311](https://doi.org/10.1103/PhysRevC.107.044311)**I. INTRODUCTION**

Nuclear matter, an ideal infinite system made of strongly interacting nucleons, is currently subject to intense study from multiple perspectives, due to its connections to the nuclear physics of finite nuclei [1–3], the astrophysics of neutron stars and gravitational waves [4–6], and the physics of cold Fermi gases [7,8].

Nuclear matter has been studied theoretically both within *ab initio* theory and density functional theory (DFT). In short, *ab initio* or first-principle methods aim at finding an exact or systematically improvable solution to the many-body problem starting from a Hamiltonian that describes the interactions among the constituent nucleons [9–11]. DFT, on the other hand, maps the many-particle problem to a single-particle (s.p.) self-consistent (s.c.) problem that is based on the concept of an energy density functional (EDF), i.e., on expressing the total energy of a generic system as a functional of its (generalized) densities [12–14]. DFT is in principle an exact theory, but the EDF which are currently used rely heavily on phenomenology [13].

The equation of state (EOS), i.e., (at zero temperature) the energy per particle as a function of the neutron and proton densities, is the fundamental ground state (g.s.) property of homogeneous matter and has been the main target of most works, see the reviews in Refs. [1,5,15]. Another line of research has focused on inhomogeneous nuclear matter [8], motivated by the fact that the inner crust of neutron stars is not uniform [4] and by the attractive possibility of constraining specific terms of the nuclear EDFs (see, e.g., Refs. [16–19]). Neutron and neutron-proton drops, i.e., nuclear matter confined by an external trap, have been studied,

e.g., in Refs. [16,20–22]. The problem of the response of nuclear matter subject to a weak periodic perturbation has also been tackled. The dynamical response function has been determined for rather general EDFs numerically [23] and analytically (see Refs. [24,25] and references therein). Recently, Gezerlis and collaborators [26–28], extending techniques used for the electron gas [29–31] and cold atoms [32], have attacked the problem of the neutron matter static response *ab initio* with the auxiliary field diffusion Monte Carlo (AFDMC) method [33,34].

While the EOS and the static and dynamic response can be studied directly in the thermodynamic limit (TL) in the framework of DFT [1,24], most *ab initio* methods simulate infinite matter by employing a finite number of particles (see, e.g., Refs. [9,35–39]). In fact, they are limited to few tens of fermions at most, which implies that *ab initio* results are affected by finite-size (FS) effects. In this context, developing a finite-*A* DFT formalism for nuclear matter is important for two reasons. First, very large numbers of particles can be studied in DFT due to its low computational cost and thus a playground for understanding and handling FS effects is provided. For example, Gezerlis *et al.* have presented a DFT method for perturbed neutron matter in Ref. [40] and used it in Ref. [28] to extrapolate their $N = 66$ AFDMC simulations [27] to the TL. Second, the finite-*A* DFT approach is instrumental in our program of constructing *ab initio* based EDFs started in Ref. [41], since it paves the way to matching *ab initio* and DFT calculations with the same number of particles in a consistent manner. The EOS of uniform matter has already been employed in a local density approximation scheme [23,41] to link the EDF to microscopic theory. Full-fledged EDFs, however, must incorporate surface terms that can act exclusively in nonuniform systems. Perturbed nuclear matter, in this respect, is a promising candidate for setting constraints on the EDF surface contribution (see, e.g., Refs. [8,32,42]).

*francesco.marino@unimi.it

This work is devoted to a detailed description of the solution of the DFT problem for nuclear matter under the effect of an external perturbation for Skyrme-like EDFs. Our approach, which represents an extension of that of Ref. [40], is based on simulating nuclear matter using a finite number of nucleons in a box on which periodic boundary conditions are imposed. The formalism for pure neutron matter (PNM) and symmetric nuclear matter (SNM), together with its numerical implementation, are presented; a careful analysis of the treatment of spin-orbit is provided. The static response problem is then tackled with this method and the effect of the perturbation on the energies, densities, and level structure of the system is investigated.

This paper is structured as follows. Section II is devoted to a detailed description to the finite- A nuclear DFT formalism and to its numerical implementation. Section III reviews the theory of the static response of homogeneous matter. Results are presented in Sec. IV. Lastly, Sec. V summarizes our work and presents future developments.

II. NUCLEAR DFT FORMALISM

A. Overview of nuclear DFT

We give a brief overview of nuclear DFT [12,13]. Details are given in our previous work Ref. [41] and references therein.

We consider quasilocal (or Skyrme-like) EDF models [12] for time-reversal-invariant systems, such as spin-saturated nuclear matter, and neglect pairing. We adopt the Kohn-Sham (KS) scheme [14], in which a representation in terms of s.p. orbitals $\psi_j(\mathbf{x})$ is introduced and the kinetic energy term is equal to that of a noninteracting Fermi system. Then, the total energy of a generic system is written as a functional of number density $\rho_t(\mathbf{x})$, kinetic density $\tau_t(\mathbf{x})$, and spin-orbit density $\mathbf{J}_t(\mathbf{x})$ (see Appendix A 3 for their definitions) with $t = 0, 1$ labeling isoscalar ($\rho_0 = \rho_n + \rho_p$) and isovector ($\rho_1 = \rho_n - \rho_p$) quantities, and has the following structure:

$$E = \int d\mathbf{x} \mathcal{E}(\mathbf{x}) = E_{\text{kin}} + E_{\text{pot}} + E_{\text{ext}}, \quad (1)$$

which comprises the kinetic energy, a nuclear potential energy term, and possibly an external potential contribution,

$$E_{\text{kin}} = \int d\mathbf{x} \mathcal{E}_{\text{kin}}(\mathbf{x}) = \int d\mathbf{x} \frac{\hbar^2}{2m} \tau_0(\mathbf{x}), \quad (2)$$

$$E_{\text{pot}} = \int d\mathbf{r} \mathcal{E}_{\text{pot}}(\mathbf{x}), \quad (3)$$

$$E_{\text{ext}} = \sum_{t=0,1} \int d\mathbf{x} \rho_t(\mathbf{x}) v_t(\mathbf{x}). \quad (4)$$

Throughout this work \mathcal{E}_{pot} has the form [41]

$$\begin{aligned} \mathcal{E}_{\text{pot}}(\mathbf{x}) = \sum_{t=0,1} \left(\sum_{\gamma} (c_{\gamma,0} + c_{\gamma,1} \beta^2) \rho_0^{\gamma+1} + C_t^t \rho_t \tau_t \right. \\ \left. + C_t^{\Delta\rho} \rho_t \Delta\rho_t + C_t^J \mathbf{J}_t^2 + C_t^{\nabla J} \rho_t \nabla \cdot \mathbf{J}_t \right) \end{aligned} \quad (5)$$

with $\beta = \rho_1/\rho_0$ being the isospin asymmetry. The KS-DFT equations are found by minimizing the EDF with respect to the s.p. orbitals $\psi_j^*(\mathbf{x})$ and read for protons and neutrons ($q = n, p$) [12]

$$\begin{aligned} \left[-\nabla \cdot \frac{\hbar^2}{2m_q^*} \nabla + U_q(\mathbf{x}) + v_q(\mathbf{x}) \right. \\ \left. + \mathbf{W}_q(\mathbf{x}) \cdot (-i)(\nabla \times \sigma) \right] \psi_j(\mathbf{x}) = \epsilon_j \psi_j(\mathbf{x}), \end{aligned} \quad (6)$$

where the fields entering the equations are defined as

$$U_q = \frac{\delta E}{\delta \rho_q}, \quad \frac{\hbar^2}{2m_q^*} = \frac{\delta E}{\delta \tau_q}, \quad \mathbf{W}_q = \frac{\delta E}{\delta \mathbf{J}_q}. \quad (7)$$

$m_q^*(\mathbf{x})$, $U_q(\mathbf{x})$, and $\mathbf{W}_q(\mathbf{x})$ are called effective mass, mean field, and spin-orbit potential, respectively.

B. Infinite nuclear matter

Nuclear matter is an infinite system of nucleons that interact through the strong interaction only [1,43]. In the following we concentrate on zero-temperature and spin-unpolarized matter. Moreover, we limit ourselves to the limiting cases of SNM ($\rho_n = \rho_p = \rho_0/2$) and PNM ($\rho_p = 0$, $\rho_n = \rho_0$), although extensions are straightforward. The fundamental quantity that characterizes homogeneous matter is the EOS $e(\rho, \beta) = E(\rho, \beta)/A$, where E is the total energy of the system and e the energy per nucleon. We also remind that in homogeneous matter both the gradients of the density and the spin-orbit density vanish [41].

Some theoretical approaches attack nuclear matter directly in the TL. These include nuclear DFT [1,24] and, e.g., self-consistent Green's functions [44]. Most *ab initio* methods, though, simulate infinite matter by using a finite number of particles (see, e.g., Refs. [35,36,39]). Among them is AFDMC [34], that has been used extensively not only for the nuclear matter EOS, but also for inhomogeneous matter, namely neutron drops [16], as well as for neutron matter response [27]. DFT, too, can be formulated with a finite nucleon number, as proposed in Ref. [40]. The standard technique adopted in most studies [34,35] involves considering A fermions enclosed in a cubic box of size L and volume $\Omega = L^3$ and imposing periodic boundary conditions (PBCs) on the wave function. The cell size is chosen such as the density of the system is a fixed and constant $\rho_0 = A/\Omega$. In this framework, the TL corresponds to the limit in which both A and L go to infinity while keeping ρ_0 fixed [43]. The free gas (FG), that is the starting point for studying interacting matter, is described in terms of s.p. plane waves orbitals $e^{i\mathbf{k}\cdot\mathbf{x}}/\sqrt{\Omega}$ with wave number \mathbf{k} and kinetic energy $\frac{\hbar^2 \mathbf{k}^2}{2m}$. As a consequence of PBCs, the momenta \mathbf{k} are quantized, i.e., $\mathbf{k} = \frac{2\pi}{L} \mathbf{n}$ where \mathbf{n} is a three-component vector of integer numbers. Since the energy depends on \mathbf{k}^2 and thus on \mathbf{n}^2 , a ‘‘momentum space’’ shell structure emerges, with different energy levels being labeled by n^2 and being degenerate. The first few momentum space ‘‘magic numbers’’ are given by $A/g = 1, 7, 19, 27, 33$, etc. [35], where g is spin/isospin degeneracy (2 for spin-saturated PNM, 4 for spin-saturated SNM). Typically, the number of fermions in a

calculation is selected so as to correspond to a shell closure of the FG in both homogeneous and perturbed matter. As we discuss below, this choice is fundamental when calculating the EOS with finite- A methods.

C. Solution of DFT in a periodic box

We discuss in detail the solution of the DFT problem for a finite number of nucleons enclosed in a cubic box with PBCs. We focus on spin-saturated PNM and SNM, which are the most important cases for nuclei and neutron stars [1]. Moreover, SNM and PNM can be treated as two-component (spin up/down) fermionic systems in a unified way. The case of asymmetric matter ($\rho_n \neq \rho_p$, $N \neq Z$) would require some limited extensions of the formalism and is left for future studies. From now on, for the sake of simplicity in the notation the isospin labels (q or t) are suppressed. Our method extends the one introduced in Ref. [40], which was limited to PNM and neglected spin-orbit terms.

We consider an external potential $v(z)$ that is a function of the z coordinate only. Thus, translational invariance is broken in the z direction, but still holds in the xy plane. In order to respect PBCs, $v(z)$ must be periodic as well. Moreover, we adopt the spin- and isospin-independent sinusoidal potential

$$v(z) = 2v_q \cos(qz) \quad (8)$$

with q being an integer multiple of $q_{\min} = 2\pi/L$. The s.p. wave functions (in two-spinor notation), then, have the following structure:

$$\psi_{\mathbf{n},\lambda}(\mathbf{x}) = \frac{e^{ik_x x} e^{ik_y y}}{\sqrt{L} \sqrt{L}} \begin{pmatrix} \phi_{\mathbf{n},\lambda}(z, \uparrow) \\ \phi_{\mathbf{n},\lambda}(z, \downarrow) \end{pmatrix} \quad (9)$$

PBCs imply that k_x and k_y are quantized in units of $2\pi/L$, i.e., $k_x = \frac{2\pi}{L}n_x$ and $k_y = \frac{2\pi}{L}n_y$, and $\phi_{\mathbf{n},\lambda}(z)$ is periodic, i.e., $\phi_{\mathbf{n},\lambda}(z+L) = \phi_{\mathbf{n},\lambda}(z)$. The states are labeled by the three integer numbers \mathbf{n} , plus a spin quantum number $\lambda = \pm 1$ whose precise meaning will be discussed below.

The general DFT equations (6) are now specialized to our case. We first note that the fields are functions of the z coordinate only: $m^* = m^*(z)$, $U = U(z)$ and $\mathbf{W} = W(z)\hat{\mathbf{z}}$. (The detailed expressions of the EDF and the fields are reported in Appendix A.1.) For later convenience, we define the transverse momentum as

$$\mathbf{k}_{n_x n_y} = k_x \hat{\mathbf{x}} + k_y \hat{\mathbf{y}} = \frac{2\pi}{L}(n_x \hat{\mathbf{x}} + n_y \hat{\mathbf{y}}) \quad (10)$$

having magnitude

$$k_{n_x n_y} = \sqrt{k_x^2 + k_y^2} = \frac{2\pi}{L} \sqrt{n_x^2 + n_y^2}. \quad (11)$$

Now, we discuss the spin-orbit term of Eq. (6) with the help of $\frac{\partial \psi_{\mathbf{n},\lambda}}{\partial x} = ik_x \psi_{\mathbf{n},\lambda}$ and $\frac{\partial \psi_{\mathbf{n},\lambda}}{\partial y} = ik_y \psi_{\mathbf{n},\lambda}$:

$$\begin{aligned} \mathbf{W}(\mathbf{x}) \cdot (-i)(\nabla \times \sigma) \psi_{\mathbf{n},\lambda}(\mathbf{x}) &= W(z)(-i)(\partial_x \sigma_y - \partial_y \sigma_x) \psi_{\mathbf{n},\lambda}(\mathbf{x}) \\ &= W(z)(k_x \sigma_y - k_y \sigma_x) \psi_{\mathbf{n},\lambda}(\mathbf{x}) \\ &= W(z) K_{n_x, n_y} \psi_{\mathbf{n},\lambda}(\mathbf{x}). \end{aligned} \quad (12)$$

In the last equality, we have introduced the spin matrix $K_{n_x, n_y} = k_x \sigma_y - k_y \sigma_x$, which reads explicitly as

$$K_{n_x, n_y} = \begin{pmatrix} 0 & -i(k_x + ik_y) \\ i(k_x - ik_y) & 0 \end{pmatrix}. \quad (13)$$

Since K_{n_x, n_y} is not diagonal, it is clear that the states $\psi_{\mathbf{n},\lambda}$ cannot be eigenstates of σ_z . While one possibility would be to solve the coupled DFT equation for the spin-up and -down components, a better choice is to take the ψ 's to be eigenstates of K_{n_x, n_y} , as suggested in Ref. [45]. It is easy to verify that K_{n_x, n_y} has eigenvalues $\pm k_{n_x, n_y}$. Thus we impose

$$K_{n_x, n_y} \psi_{\mathbf{n},\lambda}(\mathbf{x}) = \lambda k_{n_x, n_y} \psi_{\mathbf{n},\lambda}(\mathbf{x}), \quad (14)$$

where $\lambda = \pm 1$. Importantly, since K_{n_x, n_y} is independent of the position, Eq. (14) implies that the orbitals (9) can be decomposed into the product of a single spatial orbital and a constant spinor, namely,

$$\psi_{\mathbf{n},\lambda}(\mathbf{x}) = \frac{e^{ik_x x} e^{ik_y y}}{\sqrt{L} \sqrt{L}} \phi_{\mathbf{n},\lambda}(z) \chi_{n_x, n_y, \lambda}. \quad (15)$$

The spinors $\chi_{n_x, n_y, \lambda}$ satisfy

$$K_{n_x, n_y} \chi_{n_x, n_y, \lambda} = \lambda k_{n_x, n_y} \chi_{n_x, n_y, \lambda}, \quad (16)$$

where

$$\chi_{n_x, n_y, \lambda} = \frac{1}{\sqrt{2}} \begin{pmatrix} 1 \\ \lambda e^{i\phi} \end{pmatrix}. \quad (17)$$

In the last expression, the angle ϕ is given by $\phi = \arctan(n_y/n_x)$.

Physically, the states $\psi_{\mathbf{n},\lambda}$ have a definite spin projection in the direction of the transverse momentum (10), which is not fixed but depends on the numbers n_x, n_y . The label λ thus can be interpreted as a spin projection or helicity quantum number.

The kinetic term can be manipulated along the same lines and is discussed in Appendix A.2. Finally, applying Eqs. (A11), (12), and (14) to Eq. (6), we find the following one-dimensional equations for the spatial orbital $\phi_{\mathbf{n},\lambda}(z)$:

$$\begin{aligned} -\frac{d}{dz} \left(\frac{\hbar^2}{2m^*(z)} \phi'_{\mathbf{n},\lambda}(z) \right) &+ \left(U(z) + v(z) + \lambda k_{n_x, n_y} W(z) + \frac{\hbar^2}{2m^*(z)} k_{n_x, n_y}^2 \right) \phi_{\mathbf{n},\lambda}(z) \\ &= \epsilon_{\mathbf{n},\lambda} \phi_{\mathbf{n},\lambda}(z). \end{aligned} \quad (18)$$

These are s.p. state-dependent Schrödinger equations that must be solved self-consistently due the density-dependence of the fields. For a given set of quantum numbers n_x, n_y and λ , n_z labels the eigensolutions ordered by increasing s.p. energies ϵ . The z coordinate is restricted to the symmetric interval $[-\frac{L}{2}, \frac{L}{2}]$.

We note that due to time-reversal invariance, that holds if we consider the spin-independent potential (8), the eigenvalues $\epsilon_{\mathbf{n},+1}$ and $\epsilon_{\mathbf{n},-1}$ are degenerate, while in general $\lambda = \pm 1$ spatial orbitals are different. In the special case of homogeneous matter [$v = 0$ and $\rho(z) = \rho_0$], though, the spin-orbit field $W(z)$ vanishes [see Eq. (A8)], and thus the equations for

the spin-orbit partners $\lambda = \pm 1$ are identical and so are the orbitals, namely $\phi_{n,+1} = \phi_{n,-1}$. As a consequence, the spin-orbit density vanishes too [Eq. (A14)] and thus uniform matter is insensitive to spin-orbit. In passing, we also observe that the energy of a spin-saturated and closed-shell system is invariant when the sign of the spin-orbit coefficient is flipped, $C^{\nabla J} \rightarrow -C^{\nabla J}$. Indeed, the effect of this transformation is that of swapping the $\lambda = 1$ and $\lambda = -1$ states in Eq. (18) and, if an equal number of spin states is occupied, all the densities, including $J(z)$, remain unchanged, and so does the total energy.

We shall describe how the Schrödinger equation (18) is solved, how the many-particle g.s. of the system is constructed, and how the s.c. loop is dealt with. Due to the intrinsic periodicity of the systems under study, expanding Eq. (18) in the plane waves basis (see, e.g., Refs. [14,46]) allows to solve the problem very efficiently. A few tens of plane waves are typically enough to find converged results even for moderately strong perturbations; by contrast, the finite-difference approach used in Ref. [40] requires a mesh of several hundreds of points at least and a much more time-consuming diagonalization. The orbitals are Fourier-expanded as $\phi(z) = \frac{1}{\sqrt{L}} \sum_k c_k e^{ikz}$, where again $k = \frac{2\pi}{L}n$ and the Schrödinger equation is recast into matrix form, namely,

$$\sum_{k'} (\tilde{h}_{n,\lambda})_{k,k'} c_{k'} = \epsilon_{n,\lambda} c_k, \quad (19)$$

where $(\tilde{h}_{n,\lambda})_{k,k'}$ is the Hamiltonian matrix in the plane waves basis and is derived in Appendix A 4.

Nuclear DFT is based on an independent-particle picture and the many-particle g.s. configuration is found by occupying the first A energy levels of the system. In order to determine them, Eqs. (18) are solved for several different combinations (n_x, n_y) , and separately for the two spin states λ [40]. Then, the solutions are collated and the lowest-energy states are filled up with $A/2$ spin-up and $A/2$ spin-down particles. (The discussion is limited to spin-saturated system.) Energy levels are degenerate, since n_x and n_y only enter Eq. (18) in the combination $k_{n_x n_y} \propto n_x^2 + n_y^2$, so that inverting the sign of n_x , n_y or both, or exchanging the two numbers, leaves the equation invariant. Such degeneracy $g_{n_x n_y}$ can be exploited to reduce the computational load of the method, since we can restrict ourselves to the pairs (n_x, n_y) with $0 \leq n_x \leq n_y \leq n_{\max}$. It is good practice to choose at first a large value for n_{\max} , though the following argument, which generalizes that of Ref. [40], allows to stop the search over the (n_x, n_y) pairs sooner. Indeed, we observe that $k_{n_x n_y}$ enters Eq. (18) in the combination $\lambda k_{n_x n_y} W(z) + \frac{\hbar^2}{2m^*(z)} k_{n_x n_y}^2$. This contribution is positive when $k_{n_x n_y}$ satisfies the inequality

$$k_{n_x n_y} > \bar{k}_{n_x n_y} = \max_z \left(-\lambda \frac{2m^*(z)W(z)}{\hbar^2} \right). \quad (20)$$

Then, provided that $k_{n_x n_y} > \bar{k}_{n_x n_y}$, the lowest eigenvalue of Eqs. (18) increases as $k_{n_x n_y}$ increases. Now, while one is iterating over the combinations (n_x, n_y) (which must have been sorted according to increasing values of $n_x^2 + n_y^2$), and separately for $\lambda = +1$ and -1 , one checks whether the lowest eigenvalue $\epsilon_{n_x, n_y, 0, \lambda}$ is greater than the energy of the first $A/2$

lowest-energy states found so far. In that case, the cycle can be stopped, since we are guaranteed by Eq. (20) that the many-nucleon g.s. does not receive contributions from higher $n_x^2 + n_y^2$.

Once the occupied orbitals and the corresponding s.p. energies have been found, the total energy and the densities (Appendix A 3) of the system are computed.

The total energy is evaluated in two ways, i.e., as an integral of the energy density,

$$E = L^2 \int_{-L/2}^{L/2} dz \mathcal{E}(z), \quad (21)$$

and by means of

$$E = \frac{1}{2} \left(T + \sum_j \epsilon_j \right) + E_{\text{rea}}. \quad (22)$$

The rearrangement energy E_{rea} and the energy density $\mathcal{E}(z)$ are given in Appendix A 1. The expressions (21) and (22) must match when they are evaluated on the g.s. and this provides a strong check on the correctness of the method and on its convergence to the exact g.s.

A crucial aspect of DFT is that the potential is itself a functional of the densities. Therefore, a s.c. solution to the problem must be looked for [12]. At each iteration i of the s.c. loop, the densities are determined for the current values of the fields, as described above. Then new fields are generated by linearly mixing the old fields with the ones evaluated on the newly obtained densities $\rho^{(i)}$ [47], namely,

$$U^{(i+1)} = \alpha U^{(i)} + (1 - \alpha) U[\rho^{(i)}] \quad (23)$$

and similar relations for W and $\hbar/(2m^*)$. α is a mixing parameter; in order to achieve convergence, it is safe to be rather conservative, e.g., we choose $\alpha = 0.8-0.9$ at the beginning and then gradually decrease it as iterations go by. At the beginning ($i = 0$), the densities are initialized at the uniform matter values $\rho(z) = \rho_0$, $\tau(z) = \frac{3}{5} \rho_0 q_F^2$, and $J(z) = 0$ and the fields are determined accordingly.

The s.c. procedure is stopped if two conditions are met: the energies between iterations i and $i - 1$ and, at the same time, the two formulas (22) and (21) for the energy at iteration i , agree within a chosen tolerance. Thresholds of the order of 0.1–1 keV per nucleon can be obtained usually in few tens of iterations. Combining linear mixing and two convergence conditions makes our approach rather robust.

III. THEORY OF THE STATIC RESPONSE

The theory of the response of homogeneous matter to an external static perturbation is summarized. In-depth discussions can be found in Refs. [30,48,49].

Consider a system with uniform g.s. density ρ_0 , described either by a Hamiltonian \hat{H} or an EDF. A static potential $v(\mathbf{x})$ coupled to the total density is then turned on. $v(\mathbf{x})$ is periodic so as to respect the PBCs. The density and energy of the g.s. of the perturbed system are called $\rho_v(\mathbf{x})$ and $E[v]$, respectively. If the external potential is weak enough, its effect can be treated perturbatively (see, e.g., Refs. [43,48]). The

density fluctuation induced by $v(\mathbf{x})$, in particular, is linear in the external potential and is written as follows:

$$\delta\rho(\mathbf{x}) = \rho_v(\mathbf{x}) - \rho_0 = \int d\mathbf{x}' \chi(\mathbf{x}, \mathbf{x}') v(\mathbf{x}'). \quad (24)$$

The static response function $\chi(\mathbf{x}, \mathbf{x}')$ has been introduced and we stress that it depends exclusively on the properties of the unperturbed system. The response of homogeneous matter, in particular, is a function only of $\mathbf{x} - \mathbf{x}'$, i.e., $\chi(\mathbf{x}, \mathbf{x}') = \chi(\mathbf{x} - \mathbf{x}')$.

While a generic periodic function $v(\mathbf{x})$ is a superposition of plane waves, in the following we consider without loss of generality a monochromatic potential oscillating at a given wave number \mathbf{q} , namely,

$$v(\mathbf{x}) = v_q e^{i\mathbf{q}\cdot\mathbf{x}} + c.c. = 2v_q \cos(\mathbf{q} \cdot \mathbf{x}). \quad (25)$$

Thus the density fluctuation induced by the perturbation (25) is monochromatic too and is given by

$$\delta\rho(\mathbf{x}) = 2\rho_q \cos(\mathbf{q} \cdot \mathbf{x}), \quad (26)$$

where the amplitude ρ_q is linear in v_q , i.e.,

$$\rho_q = \chi(q) v_q \quad (27)$$

and $\chi(q)$ is the Fourier transform of $\chi(\mathbf{x}, \mathbf{x}')$, see Eq. (B6). The energy of the perturbed system, instead, is quadratic in the external potential. In Appendix B, we derive that the energy per particle is given by [30]

$$\delta e_v = e_v - e_0 = \frac{\chi(q)}{\rho_0} v_q^2. \quad (28)$$

The formalism we have outlined is valid both in the TL and in finite systems, and both for DFT and for Hamiltonian-based methods. The question is now how to compute the response function in practice. For generalized Skyrme EDFs [24] and Gogny and Nakada EDFs [25], for example, the response in the TL can be determined analytically (Appendix C). An alternative for studying $\chi(q)$ is provided by exploiting Eq. (27) or (28). The strategy to determine $\chi(q)$ for a uniform system at a given density ρ_0 , and with a given particle number, is the following. For a given (quantized) momentum q , multiple calculations of the g.s. of the perturbed system are performed for different values of the strength v_q of the external potential (25). Then $\chi(q)$ can be extracted from the amplitude of the density fluctuations [Eq. (27)] or from the energies [Eq. (28)] as a function of v_q , for sufficiently small v_q . This strategy has been applied in several contexts, e.g., Refs. [27,30,50,51], and provides a relatively straightforward way to determine the static response function numerically.

In the following, we will extract $\chi(q)$ by interpolating energies with the more general formula [27,50]:

$$\delta e_v = e_v - e_0 = \frac{\chi(q)}{\rho_0} v_q^2 + C_4 v_q^4 \quad (29)$$

which takes into account higher-order contributions. In Appendix D, we discuss the extraction of $\chi(q)$ from the fit of density fluctuations via Eq. (27). Therein, we also show and explain why very close results are found by means of the two techniques.

Second-order perturbation theory, or equivalently the spectral representation of the dynamical density response $\chi(\mathbf{q}, \omega)$, can be employed to derive a formula that relates $\chi(q)$ to the excited states of the homogeneous system [43,48]. For the case of the spin- and isospin-saturated A-fermion FG, the response $\chi_{0,A}$ at zero temperature is given by [48,50]

$$\chi_{0,A}(q) = -\frac{4mg}{\hbar^2 \Omega} \sum_{\mathbf{k}_{\text{occ}}} \frac{1}{(\mathbf{k} + \mathbf{q})^2 - \mathbf{k}^2}, \quad (30)$$

where the sum extends over the occupied momentum states and terms with vanishing denominator are can be safely neglected. Consistently with the assumptions of Sec. II, we write $\mathbf{k} = \frac{2\pi}{L} \mathbf{n}$ and take \mathbf{q} quantized and parallel to the z direction, i.e., $\mathbf{q} = q\hat{\mathbf{z}} = \frac{2\pi}{L} p\hat{\mathbf{z}}$, with p integer. Then Eq. (30) is expressed as

$$\chi_{0,A}(q) = -\frac{mg}{L\pi^2 \hbar^2} \sum_{\mathbf{n}_{\text{occ}}} \frac{1}{p^2 + 2pn_z}. \quad (31)$$

This formula is straightforward to evaluate: we determine the occupied states of the A-particle FG g.s. once and then, for each value of q , we simply perform a sum over these states. In the TL, $n_{\mathbf{k}} = \theta(q_F - k)$, $\frac{1}{\Omega} \sum_{\mathbf{k}} \rightarrow \int \frac{d\mathbf{k}}{(2\pi)^3}$ [43] and the static response becomes the well-known Lindhard function at zero-frequency [52]

$$\chi_0(q) = -g \frac{mq_F}{2(\hbar\pi)^2} f\left(\frac{q}{2q_F}\right), \quad (32)$$

$$f(k) = \frac{1}{2} \left(1 + \frac{1-k^2}{2k} \log \left| \frac{1+k}{1-k} \right| \right). \quad (33)$$

IV. RESULTS

The method described in Sec. II is applied to calculate the EOS and the static response. The popular SLy4 EDF [53] is used when not stated otherwise, and examples of perturbed matter calculations are typically performed at a reference density of $\rho_0 = 0.16 \text{ fm}^{-3}$. DFT energies are converged within a tolerance of 1 keV per nucleon. Perturbation strengths are measured in units of the Fermi energy of the corresponding system (v_q/E_F). We plot the static response function in the form $-\chi(q)/\rho_0$ (in MeV^{-1}), which is everywhere positive. Momenta are reported either in units of the Fermi momentum (q/q_F) or as integer multiples of the minimum allowed momenta ($q_{\min} = 2\pi/L$).

A. EOS

As a first application, the EOS is studied in both SNM (Fig. 1) and PNM (Fig. 2). The TL EOS is shown as a solid line, while calculations with $A = 132$, 16676 nucleons and $N = 66$, 8338 neutrons, respectively, are reported as symbols. Multiples of 33 particles are commonly used in infinite matter studies, because the kinetic energy per particle of FG made of 33g particles is rather close to TL FG energy (see Ref. [27], Fig. 1). As a prototypical large- A system, we use a number of nucleons equal to 4169 times the spin/isospin degeneracy g , which corresponds to filling up all the momentum shells of the FG up to $n^2 = n_x^2 + n_y^2 + n_z^2 = 100$. Moreover, the insets

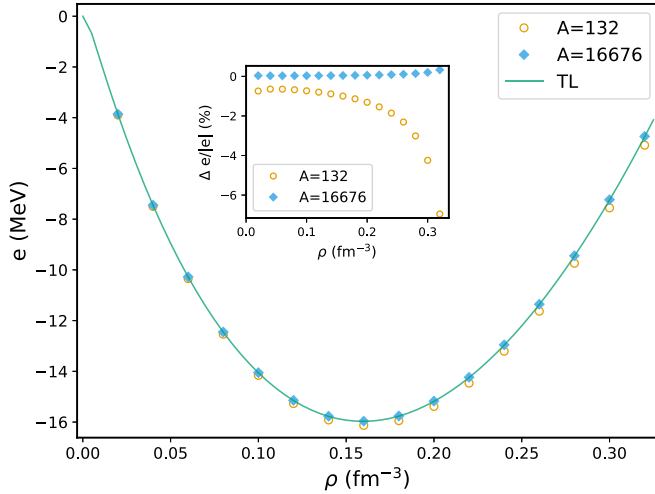


FIG. 1. SNM EOS computed with the SLy4 EDF in the TL (line) and with a finite number of particles (symbols). Inset: relative difference (in percentage) between the finite- A and TL EOS as a function of the density.

in Figs. 1 and 2 show the relative difference (in percentage) between the finite- A and TL EOS as a function of the density ($\Delta e/|e| = (e_A - e_{TL})/|e_{TL}|$). Indeed, the results of the large- A calculations turn out to be practically indistinguishable from the TL curve and provide a strong check on the correctness of numerical calculations. It can also be appreciated that the $N = 66$ and $A = 132$ EOS give energies rather close to the TL EOS. Discrepancies amount to no more than 2% in PNM over the considered range of densities. In SNM they remain within 2% up to $\rho = 0.26 \text{ fm}^{-3}$, then they display a tendency to grow as the density further increases. At twice the saturation density, the difference has increased to roughly 6%. We suggest that the larger FS effects in SNM compared to PNM are a consequence of the stronger interactions in SNM. That is, choosing $A = 33g$ allows to approximate the TL kinetic energy effectively at all densities, but some FS effects on the potential energy persist and manifest themselves mostly in the highly correlated SNM in the high density region.

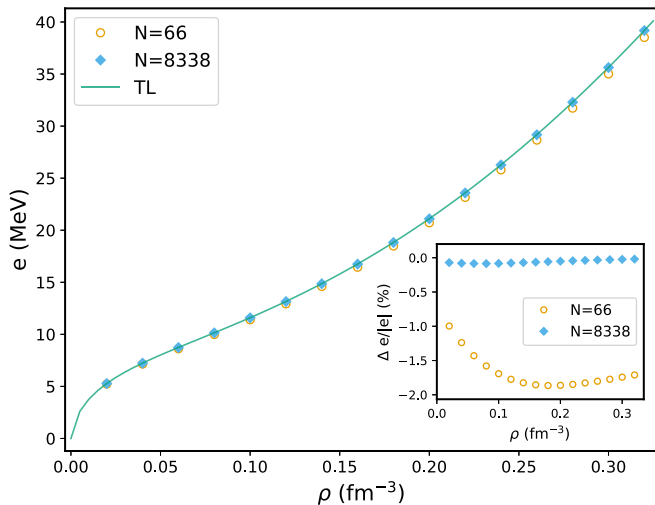


FIG. 2. Same as Fig. 1, but for PNM.

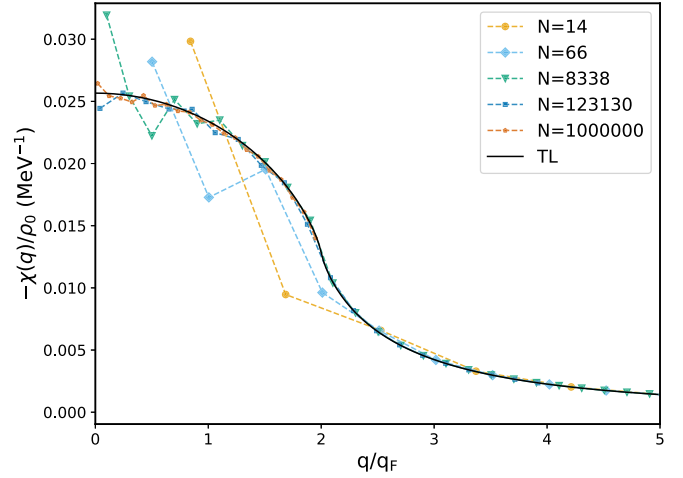


FIG. 3. Dashed lines: free response function $-\chi_{0,N}(q)/\rho_0$ in PNM at $\rho_0 = 0.16 \text{ fm}^{-3}$ as a function of q/q_F for different numbers of neutrons. Full line: response in the TL (Lindhard function).

Nonetheless, the special usefulness of the “magic numbers” $N = 66$ and $A = 132$ is overall confirmed also for DFT calculations.

B. Free response

A second study concentrates on the static response of the FG. The exact formula for $\chi_{0,N}$ [Eq. (30)] is applied in Fig. 3 for different numbers of neutrons and compared to the TL response (32). FS effects are rather strong at small or moderate momenta and manifest themselves as a non-monotonic behavior of $\chi_{0,N}(q)$ at finite N , while the TL response function is strictly decreasing in magnitude. For $q > 2q_F$, instead, the oscillations tend to disappear and the curves match rather well for all particle numbers. This qualitative change of behavior is due to geometric reasons, see, e.g., the calculation of $\chi_0(q)$ in Ref. [43]: essentially, for $q > 2q_F$ any occupied momentum state can be scattered from the g.s. (the Fermi sphere) to an empty state and thus shell effects, that strongly affect the results at small q , are ineffective. The special role of $q = 2q_F$ is also signalled by the fact that the TL Lindhard function (32) is nonanalytical at that point. Moreover, we note that the convergence to the TL as N is increased is relatively slow and mild oscillations continue to persist up to very large N . Then, the free response is computed numerically and compared to the analytical results. In particular, the FG response is determined by solving the Mathieu problem [27], i.e., the independent-particle problem of fermions subject to the external potential (8) (with the EDF potential terms turned off), for different momenta q and for strengths v_q/E_F between 0.01 and 0.1 (with a step of 0.01). Then the energy differences δe_v are interpolated with the quartic formula (29) at each q . In Fig. 4, a comparison is drawn in the case of PNM with $N = 66$ neutrons between the exact response (filled squares) and the values obtained through the fitting procedure (empty diamonds). An almost perfect agreement is obtained, with a modest discrepancy only at the lowest momentum ($q/q_F \approx 0.5$). In order to better understand this deviation, in Fig. 5 we consider the ratio between the energy variation δe_v and the square of the perturbation strength v_q as a function of v_q/E_F . The exact response is

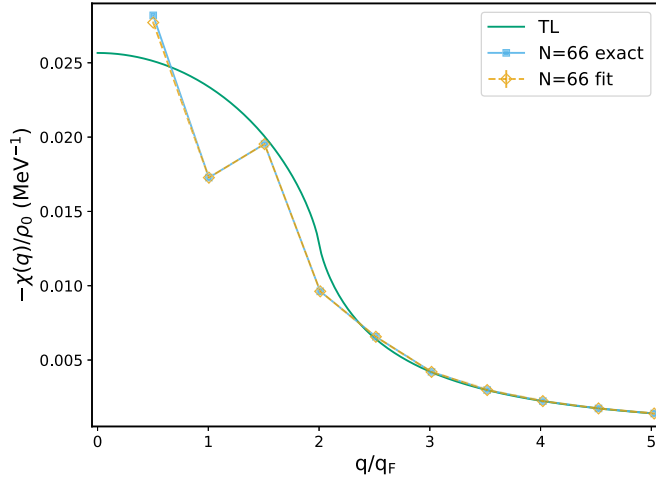


FIG. 4. Static response $-\chi_{0,N}(q)/\rho_0$ of the FG as a function of q/q_F in PNM at a density $\rho_0 = 0.16 \text{ fm}^{-3}$. The exact response (filled squares) and the response determined by a fit to the Mathieu energies (empty diamonds) are shown for $N = 66$ neutrons. For comparison, the TL response (Lindhard function) is also plotted.

shown as a hollow symbol at $v_q = 0$. If linear response theory were exact, at least in a certain range of small v_q , the ratio $\delta e_v/v_q^2$ would be constant. This is indeed verified for $q/q_{\min} > 1$ over the whole interval considered, but at $q/q_{\min} = 1$ a slight underestimation of the response is observed at all finite perturbations. This highlights that modest nonlinear (fourth-order) contributions are present in the behavior of the system. Importantly, though, the ratio correctly converges to the exact response [$\delta e_v/v_q^2 \rightarrow \chi_{0,N}(q)/\rho_0$] as $v_q \rightarrow 0$.

C. Perturbed nuclear matter

Perturbed matter is now studied with the SLy4 EDF. First, a preliminary analysis of the convergence of the

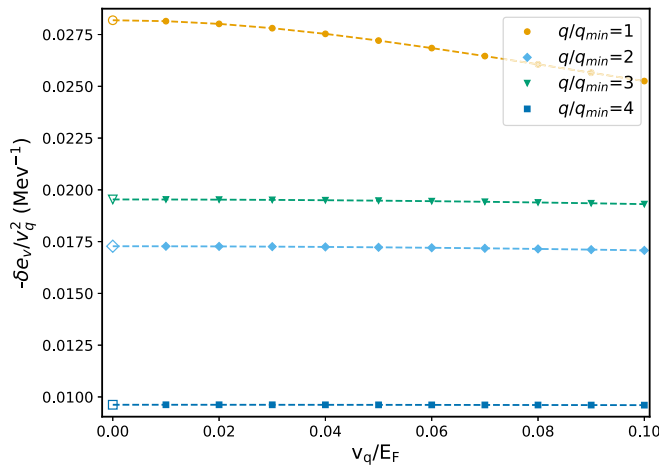


FIG. 5. Ratio between the energy variation $-\delta e_v$ and the square of the perturbation strength v_q for the first four allowed moments (q/q_{\min} between 1 and 4) for the same system as Fig. 4. Hollow symbols at $v_q = 0$ represent the exact value of $-\chi_{0,N}(q)/\rho_0$. Dashed lines are guide to the eye.

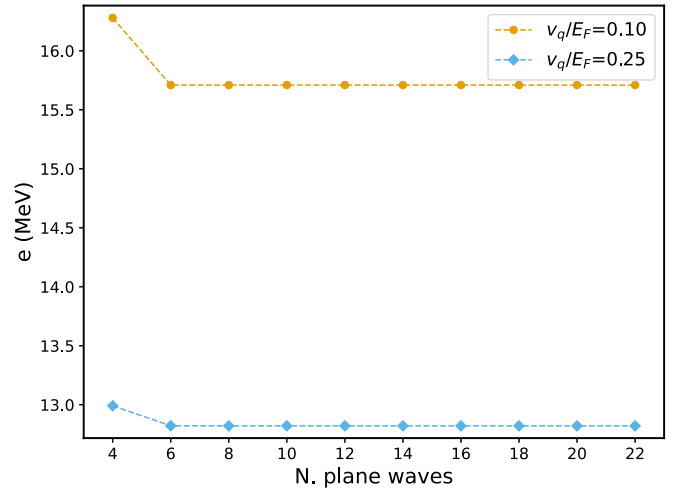


FIG. 6. Energy per particle of PNM with $N = 66$ at $\rho_0 = 0.16 \text{ fm}^{-3}$ obtained with the SLy4 EDF as a function of the number of plane waves. Results are shown for the lowest momentum ($q = q_{\min}$) for two different strengths of the external potential.

calculations with respect to the number of plane waves included in the basis is presented. Figure 6, which reports calculations performed with $N = 66$ neutrons (density $\rho_0 = 0.16 \text{ fm}^{-3}$) at $q/q_{\min} = 1$ for a small ($v_q/E_F = 0.1$) and a moderate ($v_q/E_F = 0.25$) perturbation strengths, shows that in this case as few as eight plane waves are sufficient to find energies converged within 0.1 keV or less. As a general rule, though, the number of plane waves required increases as a function of the momentum q of the perturbation and in practice we have found that a basis of 40 waves always yields converged results for 66 or 132 nucleons. When thousands of particles are considered, we raise the cutoff to 60 plane waves. Calculations remain very fast (few seconds) even on a single processor. Then, the densities $\rho(z)$ as well as their Fourier components of PNM are shown in Figs. 7 and 8, respectively,

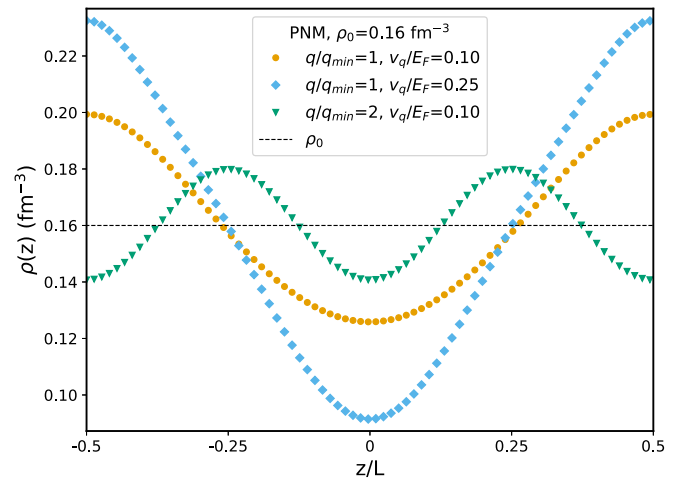


FIG. 7. Densities $\rho(z)$ as a function of z/L in PNM ($N = 66$ neutrons) at a reference density $\rho_0 = 0.16 \text{ fm}^{-3}$ (dashed horizontal line). Densities for three perturbations, differing in strength and momentum (see legend), are shown as symbols.

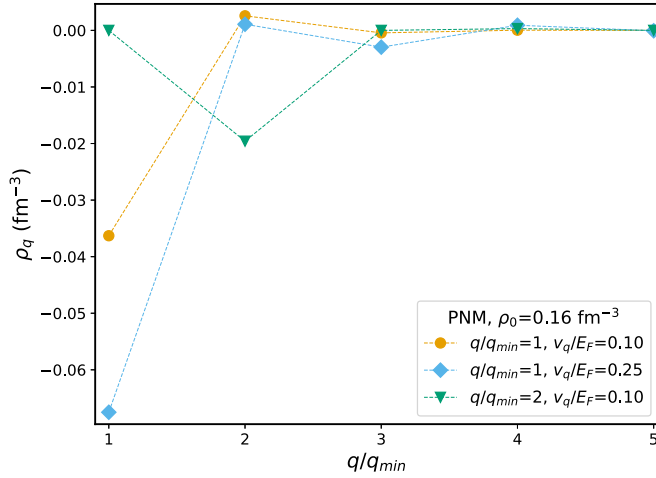


FIG. 8. Fourier components ρ_q of the density fluctuations in the same cases as Fig. 7.

for three perturbations that differ in strength and periodicity ($q/q_{\min} = 1$ with strengths $v_q/E_F = 0.1, 0.25$, and $q/q_{\min} = 2$ with $v_q/E_F = 0.1$). From the real space representation, one can appreciate that densities closely resemble cosine function that oscillate around the unperturbed density with the same periodicity as that of the external perturbation [see Eq. (26)]. The Fourier analysis confirms that the response is essentially harmonic, as in all cases a single component at momentum q is clearly dominant with rather modest contributions beyond the linear regime. For completeness, the real-space densities (Fig. 9) and their Fourier components (Fig. 10) at reference density $\rho_0 = 0.16 \text{ fm}^{-3}$ are reported for SNM ($A = 132$) too. From a qualitative point of view, the behavior of SNM is the same as that of PNM, and also the magnitude of the density fluctuation is very similar.

So far, we have always used particle numbers that correspond to a shell closure of the free Fermi gas and implicitly assumed that they are magic numbers for the perturbed system as well. This hypothesis proves true in general for weak potentials. Actually, its violation is a sign that the picture itself of a small perturbation of the homogeneous system is breaking

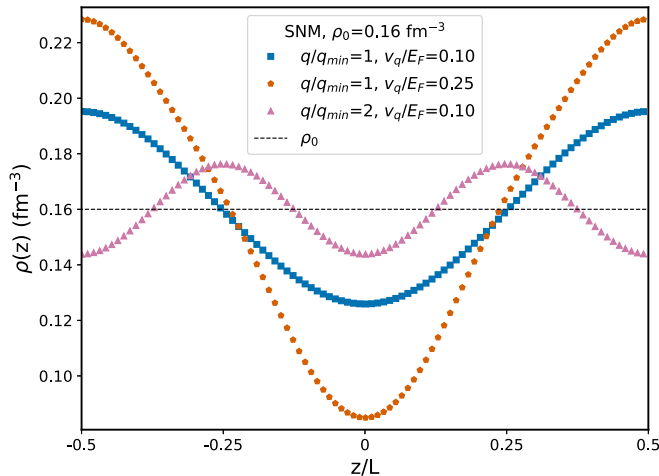


FIG. 9. Same as Fig. 7, but for SNM with $A = 132$.

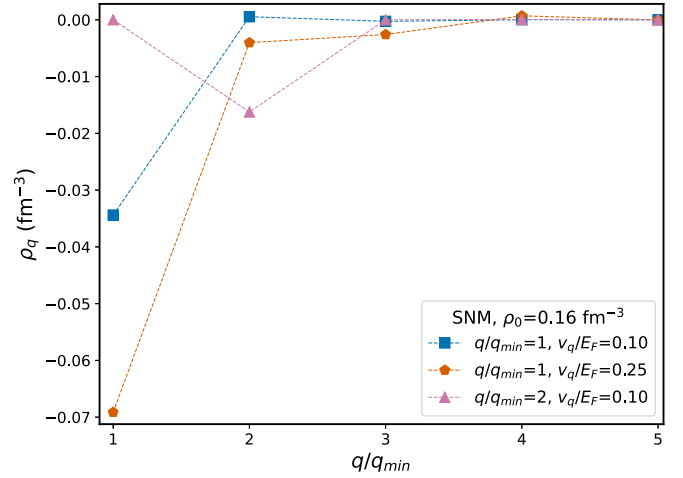


FIG. 10. Same as Fig. 8, but for SNM with $A = 132$.

down. In Fig. 11 the neutron level scheme of $N = 66$ PNM (same case as Fig. 7) is shown at two different perturbation strengths (both with momentum $q/q_{\min} = 1$). We remind that the $\lambda = \pm 1$ energy eigenvalues are degenerate and we plot the s.p. energies only for $\lambda = +1$. The quantum numbers $\mathbf{n} = (n_x, n_y, n_z)$ ($0 \leq n_x \leq n_y$), and the number of nucleons corresponding to shell closures, are reported next to each level. Among the latter, magic numbers of the FG are circled. In the case of the weaker potential, the effect of the perturbation is to partially lift the degeneracy of the free gas levels (as well as to lower the s.p. energies), as can be seen from the triplets or doublets of neighboring levels. The overall structure of the homogeneous system, though, is preserved and indeed all the FG magic numbers up to 33 are found in the perturbed system too. A markedly different picture appears for the stronger perturbation, where the level ordering of the FG is severely altered. One consequence is that a shell closure is found not for 33 nucleons but for 35. We suggest that the sudden changes in the slope of the energy as a function of the perturbation

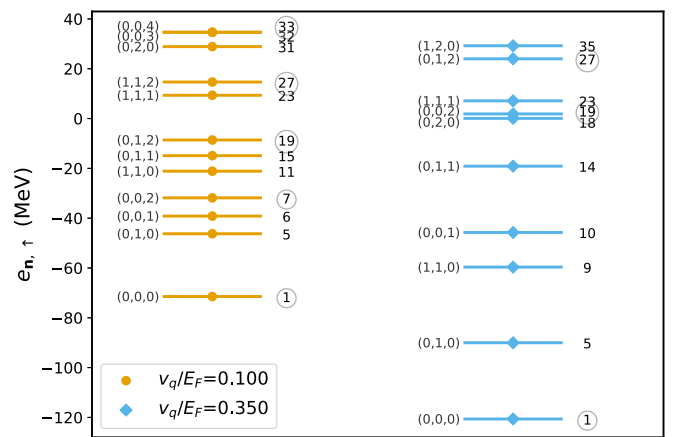


FIG. 11. Level structure of $N = 66$ PNM. Two perturbation strengths (at momentum $q/q_{\min} = 1$) are shown. The quantum numbers $\mathbf{n} = (n_x, n_y, n_z)$ of each level and the number of particles up to that shell are reported. Momentum-shell magic numbers of the FG are circled.

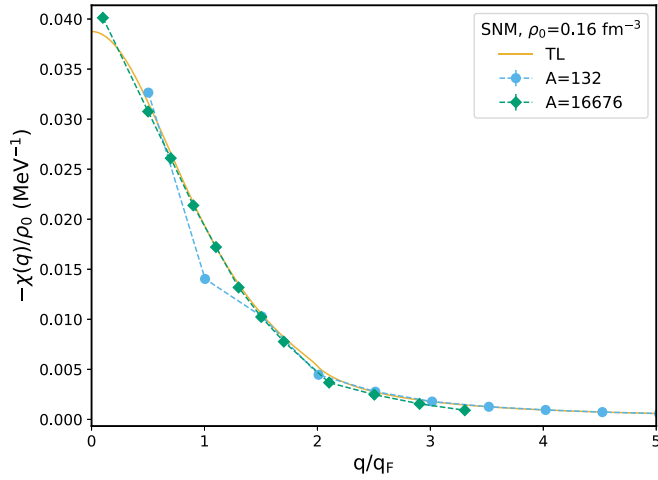


FIG. 12. Static response of SNM at $\rho_0 = 0.16 \text{ fm}^{-3}$ obtained with the SLy4 EDF. The solid line represents the TL response, while symbols denote calculations for a finite number of particles ($A = 132$ and 16676).

mentioned in Ref. [40] may be a side-effect of such ‘shell-opening’ effects. The key message is that care must be taken when studying perturbed finite- A matter and not only global properties (energy, density), but also the shell structure must be looked at. For example, we warn that, if DFT or Mathieu orbitals are used to construct a reference state for quantum Monte Carlo [27,54], it is crucial to check that it be a closed-shell state, before embarking on expensive calculations.

Next, the static response function is discussed. The TL response of nuclear EDFs is known exactly [24] (Appendix C) and is now compared to the finite- A calculations in both SNM (Fig. 12) and PNM (Fig. 13). The numerical response functions for the large- A system are in very good agreement with the analytical predictions. The convergence to the TL is thus verified and we can appreciate by comparing to Fig. 3 that it is definitely faster (as a function of the number of nucleons) in the interacting (DFT) system than for the FG. The small- A

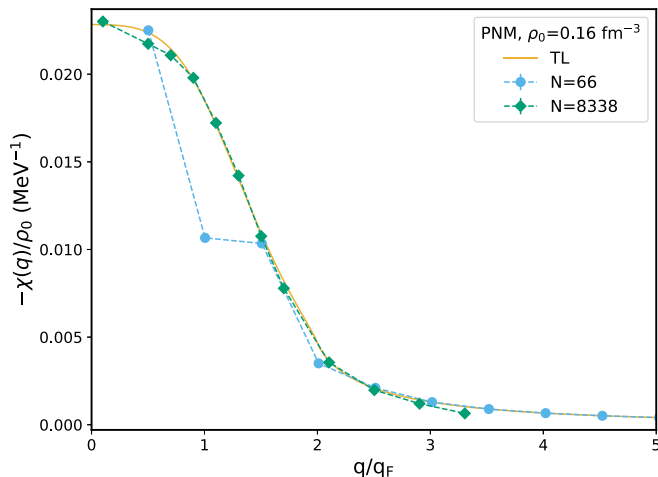


FIG. 13. Same as Fig. 12, but for PNM. Calculations are performed with $N = 66$ and 8338 neutrons (symbols) and in the TL.

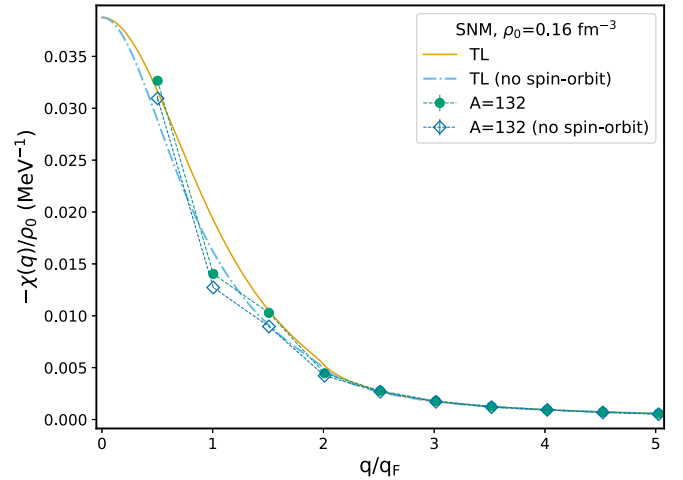


FIG. 14. SNM static response obtained in the TL and for $A = 132$ nucleons with the full SLy4 EDF and SLy4 with spin-orbit terms neglected (‘no spin-orbit’ in the legend).

response, instead, is characterized by a non-monotonic behavior that is reminiscent of that of the free response, with marked fluctuations with respect to the TL function for $q < 2q_F$. Lastly, we would like to understand the impact of the spin-orbit terms on the static response. Spin-orbit was neglected in Ref. [40] and its inclusion is one of the novelties of our work. The response computed with the full SLy4 EDF and for SLy4 with spin-orbit neglected, i.e., with $C^{\nabla J}$ set to zero, is reported for SNM (Fig. 14) and PNM (Fig. 15) both in the TL and for the usual $A = 132$ and $N = 66$ numbers of particles, respectively. One can appreciate that for the SLy4 EDF spin-orbit has the main effect of lowering the magnitude of $\chi(q)$ at all momenta, both in the TL and in the finite systems and, while in SNM it constitutes a small correction, in PNM it is a significant effect. While the qualitative picture of Ref. [40] is not altered in a fundamental way, quantitative results may change noticeably. In particular, it is important to incorporate spin-orbit terms if one aims at constraining the EDF parameters using *ab initio* information. It must be noted,

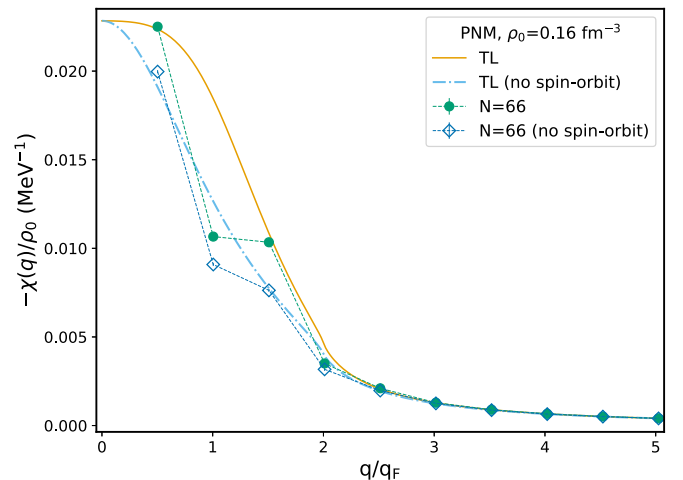


FIG. 15. Same as Fig. 14, but for PNM with $N = 66$ neutrons.

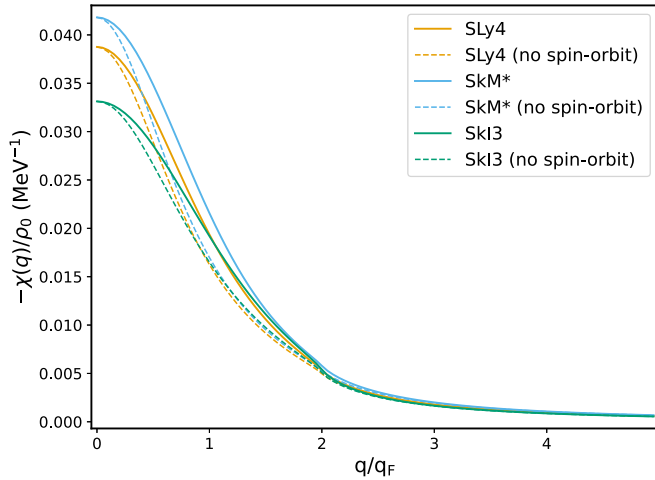


FIG. 16. TL static response in SNM at density $\rho_0 = 0.16 \text{ fm}^{-3}$ obtained with three different EDFs, both with (solid line) and without (dashed line) spin-orbit terms.

however, that the importance of the spin-orbit terms on the response is dependent on the adopted EDF, as it is apparent in the TL. A systematic analysis is outside the scope of this work, and for the purpose of demonstrating our previous assertion we show the TL response in SNM (Fig. 16) and PNM (Fig. 17) for three representative Skyrme models (SLy4 [53], SkM* [55], SkI3 [56]). While SLy4 and SkM* predict qualitatively similar response functions, SkI3 is markedly different in two respects. First, the PNM response is smaller by a factor of 2 compared to the other EDFs. The SNM response is comparable in all cases, as the isoscalar coefficients that determine the SNM response are more tightly constrained than the isovector ones that enter the PNM response [13] (Appendix A 1 and C). PNM properties can differ significantly according to the EDF, as we comment also in Appendix E. Second, in SLy4 and SkM* the spin-orbit term has a qualitative impact on the PNM response. In the SkI3, instead, it represents only a small quantitative correction in both PNM and SNM. To understand this, in Table I we have reported the isoscalar and isovector

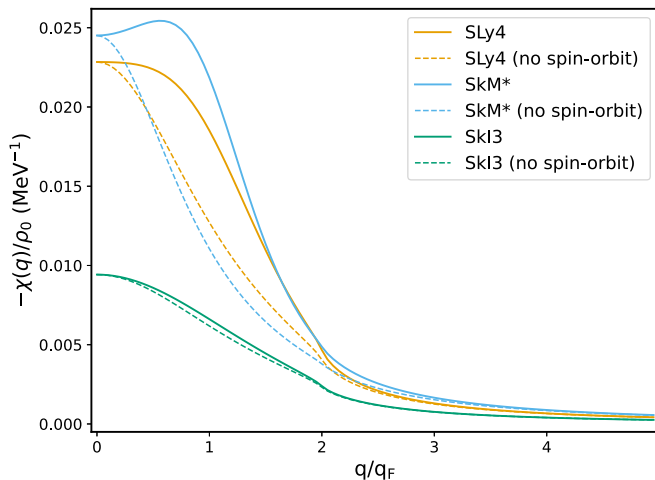


FIG. 17. Same as Fig. 16, but for PNM.

TABLE I. Spin-orbit coefficients for the SLy4, SkM*, and SkI3 EDFs. All the parameters are measured in MeV fm^5 .

EDF	$C_0^{\nabla J}$	$C_1^{\nabla J}$	$C_{nm}^{\nabla J}$
SLy4	-92.25	-30.75	-123
SkM*	-97.50	-32.5	-130
SkI3	-94.13	0	-94.13

spin-orbit coefficients, as well as the PNM coefficient $C_{nm}^{\nabla J} = C_0^{\nabla J} + C_1^{\nabla J}$ (Appendix A 1), for the three EDFs. Also, we note that the spin-orbit parameter enters the TL response quadratically in the denominator of Eq. (C11), where $X_{so} \propto C^{\nabla J}$. Then, we observe that all the three EDFs considered have roughly equal isoscalar spin-orbit coefficients. However, in SLy4 and SkM* $|C_{nm}^{\nabla J}| > |C_0^{\nabla J}|$, while in SkI3 $C_{nm}^{\nabla J} = C_0^{\nabla J}$. This may help explain why spin-orbit impacts PNM more strongly than SNM for the first two models.

V. CONCLUSIONS AND PERSPECTIVES

To sum up, in this work we have studied nuclear matter under the effect of an external potential within the DFT framework. Our approach is based on simulating nuclear matter with a finite number of nucleons enclosed in a box and subject to PBCs, and the theoretical formalism and numerical implementation have been presented in detail for PNM and SNM for Skyrme-like EDFs. We have discussed carefully how to treat spin-orbit terms and, in particular, we have shown that, although in the presence of spin-orbit the DFT orbitals are not eigenstates of the spin projection operator, single-component equations can still be derived. Then, the problem of the response of nuclear matter to static density perturbations has been analyzed with our technique.

Our method has been validated successfully by comparing the numerical results with analytical formulas for the EDF EOS, the free gas response (both for finite- A and TL systems) and the TL EDF response. The power of DFT is demonstrated by the fact that systems of thousands of particles can be computed in an extremely fast and reliable way, and the convergence to the thermodynamic limit has been verified numerically. Moreover, the validity of linear response for weak perturbations, as well as deviations occurring for stronger external potentials have been investigated by looking at energies, densities, and level structures. We point out that the momentum space magic numbers of uniform matter do not necessarily correspond to shell closures of the perturbed system. Therefore, care must be taken when the finite- A DFT approach is used in conjunction with *ab initio*, for example when DFT or Mathieu orbitals [27] are used as a reference state in quantum Monte Carlo. Moreover, in the case of the popular SLy4 EDF we have found that spin-orbit contributes significantly to the PNM response, and to a lesser extent to the SNM response. In future studies of inhomogeneous matter, therefore, spin-orbit terms should be incorporated. We should mention, however, that the impact of spin-orbit terms on the response is dependent on the chosen EDF, though a detailed study is outside the scope of this work.

This work represents an intermediate step in the program of developing *ab initio*-based EDFs started in Ref. [41]. Indeed, inhomogeneous systems are to be studied in order to gain information about the gradient terms of the EDF. Our efforts are currently devoted to the *ab initio* response of both SNM and PNM, aiming at constraining the nuclear EDF by matching DFT and *ab initio* results. In particular, our strategy involves tuning the EDF parameters on the *ab initio* energies obtained with the same number of particles so to keep FS effects under control. Results will be presented in a forthcoming publication [57].

Moreover, while here we have focused on PNM and SNM and presented results for density perturbations only, the formalism can be easily extended to isospin-asymmetric matter, as well as (introducing time-odd densities in the theory [12]) to spin-polarized matter and to spin/isospin perturbations.

ACKNOWLEDGMENTS

We thank Alessandro Lovato and Francesco Pederiva for useful discussions. F.M. acknowledges the CINECA award AbINEF (HP10B3BG09) under the ISCRA initiative, for the availability of high performance computing resources and support.

APPENDIX A: DETAILS ON NUCLEAR EDFs

Further details on the EDF and the mean fields are provided. In this work we focus on PNM and SNM, that can be treated as two-component (spin up/down) fermionic systems. We adopt the convention for which C^τ stands for C_0^τ in SNM and $C_{nm}^\tau = C_0^\tau + C_1^\tau$ in PNM, and likewise for $C^{\Delta\rho}$, $C^{\nabla J}$, and the c_γ coefficients.

1. EDFs

The expression of the EDF \mathcal{E} under the assumptions of Sec. II is the following:

$$\mathcal{E}(z) = \mathcal{E}_{\text{kin}}(z) + \mathcal{E}_{\text{bulk}}(z) + C^\tau \rho(z) \tau(z) + C^{\Delta\rho} \rho(z) \rho''(z) - C^{\nabla J} \rho'(z) J_z(z) \quad (\text{A1})$$

with

$$\mathcal{E}_{\text{kin}}(z) = \frac{\hbar^2}{2m} \tau(z), \quad (\text{A2})$$

$$\mathcal{E}_{\text{bulk}}(z) = \sum_\gamma c_\gamma \rho^{\gamma+1}(z). \quad (\text{A3})$$

The rearrangement term was computed in Ref. [41] and is given by

$$E_{\text{rea}} = L^2 \int dz \sum_\gamma \left(\frac{1-\gamma}{2} \right) c_\gamma \rho^{\gamma+1}(z). \quad (\text{A4})$$

The expressions for the mean field, effective mass, and spin-orbit potential are also shown:

$$\frac{\hbar^2}{2m^*(z)} = \frac{\hbar^2}{2m} + C^\tau \rho(z), \quad (\text{A5})$$

$$U(z) = U^{\text{bulk}}(z) + C^\tau \tau(z) + 2C^{\Delta\rho} \rho''(z) + C^{\nabla J} J_z'(z) \quad (\text{A6})$$

with

$$U^{\text{bulk}} = \sum_\gamma c_\gamma (\gamma + 1) \rho^\gamma(z), \quad (\text{A7})$$

and lastly

$$W_z(z) = -C^{\nabla J} \rho'(z). \quad (\text{A8})$$

2. Kinetic term

We derive the kinetic term of Eq. (18). First, the gradient and the Laplacian of $\psi_{\mathbf{n},\lambda}$ [Eq. (15)] are reported:

$$\begin{aligned} \nabla \psi_{\mathbf{n},\lambda}(\mathbf{x}) &= ik_x \psi_{\mathbf{n},\lambda}(\mathbf{x}) \hat{\mathbf{x}} + ik_y \psi_{\mathbf{n},\lambda}(\mathbf{x}) \hat{\mathbf{y}} \\ &+ \frac{1}{L} e^{i(k_x x + k_y y)} \chi_{n_x, n_y, \lambda} \phi'_{\mathbf{n},\lambda}(z) \hat{\mathbf{z}}, \end{aligned} \quad (\text{A9})$$

$$\begin{aligned} \nabla^2 \psi_{\mathbf{n},\lambda}(\mathbf{x}) &= -(k_x^2 + k_y^2) \psi_{\mathbf{n},\lambda}(\mathbf{x}) \\ &+ \frac{1}{L} e^{i(k_x x + k_y y)} \chi_{n_x, n_y, \lambda} \phi''_{\mathbf{n},\lambda}(z). \end{aligned} \quad (\text{A10})$$

Using these expressions, we elaborate on $-\nabla \cdot \left(\frac{\hbar^2}{2m^*} \nabla \psi_{\mathbf{n},\lambda} \right)$ as follows:

$$\begin{aligned} &-\nabla \cdot \left(\frac{\hbar^2}{2m^*(z)} \nabla \psi_{\mathbf{n},\lambda}(\mathbf{x}) \right) \\ &= -\frac{\hbar^2}{2m^*(z)} \nabla^2 \psi_{\mathbf{n},\lambda}(\mathbf{x}) - \frac{d}{dz} \left(\frac{\hbar^2}{2m^*(z)} \right) \frac{\partial \psi_{\mathbf{n},\lambda}}{\partial z} \\ &= \frac{1}{L} e^{i(k_x x + k_y y)} \chi_{n_x, n_y, \lambda} \\ &\times \left[-\frac{d}{dz} \left(\frac{\hbar^2}{2m^*(z)} \phi'_{\mathbf{n},\lambda}(z) \right) + \frac{\hbar^2}{2m^*(z)} k_{n_x, n_y}^2 \phi_{\mathbf{n},\lambda}(z) \right]. \end{aligned} \quad (\text{A11})$$

The constant spinor χ and the exponential appear in all terms in Eq. (6), thus they can be simplified and drop out of the final equations (18).

3. Densities as a function of the orbitals

Number density, kinetic density, and spin-orbit density may be computed from their definitions as functions of the occupied orbitals [12] applied to the wave functions (15). Equations (A9) and (A10) are also used to find

$$\rho(z) = \sum_j |\psi_j(\mathbf{x})|^2 = \frac{1}{L^2} \sum_{\mathbf{n},\lambda} |\phi_{\mathbf{n},\lambda}(z)|^2, \quad (\text{A12})$$

$$\begin{aligned} \tau(z) &= \sum_j |\nabla \psi_j(\mathbf{x})|^2 \\ &= \frac{1}{L^2} \sum_{\mathbf{n},\lambda} (|\phi'_{\mathbf{n},\lambda}|^2 + k_{n_x, n_y}^2 |\phi_{\mathbf{n},\lambda}|^2), \end{aligned} \quad (\text{A13})$$

$$\begin{aligned} J_z(z) &= \sum_j \psi_j^*(\mathbf{x}) (-i) (\nabla \times \sigma)_3 \psi_j(\mathbf{x}) \\ &= \sum_{\mathbf{n},\lambda} \psi_{\mathbf{n},\lambda}^*(\mathbf{x}) K \psi_{\mathbf{n},\lambda}(\mathbf{x}) \\ &= \frac{1}{L^2} \sum_{\mathbf{n},\lambda} \lambda k_{n_x, n_y} |\phi_{\mathbf{n},\lambda}(z)|^2, \end{aligned} \quad (\text{A14})$$

where only the z component of \mathbf{J} does not vanish and Eq. (16) has been used.

4. Hamiltonian in the plane waves basis

We derive the Hamiltonian matrix in the plane waves basis $(\tilde{h}_{\mathbf{n},\lambda})_{k,k'}$ [Eq. (19)]. We start from the real space DFT equations (18) and Fourier-expand the orbitals as $\phi(z) = \frac{1}{\sqrt{L}} \sum_{k'} c_{k'} e^{ik'z}$. Then, we project on the k plane wave by multiplying by e^{-ikz}/\sqrt{L} and integrating over z for $-L/2 \leq z \leq L/2$. The multiplicative terms are simple to treat and one easily finds the Fourier transform

$$\begin{aligned} \tilde{U}(k-k') &= \frac{1}{L} \int_{-L/2}^{L/2} dz e^{-i(k-k')z} \\ &\times \left(U(z) + v(z) + \lambda k_{n_x n_y} W(z) + \frac{\hbar^2}{2m^*(z)} k_{n_x n_y}^2 \right). \end{aligned} \quad (\text{A15})$$

The derivative term is slightly more involved and is discussed in detail. We simplify the notation by defining $B(z) = \frac{\hbar^2}{2m^*(z)}$ and dropping the subscripts \mathbf{n} , λ and move on to compute

$$\frac{1}{\sqrt{L}} \int_{-L/2}^{L/2} dz e^{-ikz} \left[-\frac{d}{dz} (B(z)\phi'(z)) \right]. \quad (\text{A16})$$

An integration by parts, followed by inserting $\phi'(z) = \frac{i}{\sqrt{L}} \sum_{k'} k' c_{k'} e^{ik'z}$, gives

$$\begin{aligned} &\frac{1}{\sqrt{L}} \int dz B(z)\phi'(z) \frac{d}{dz} e^{-ikz} \\ &= -i \frac{k}{\sqrt{L}} \int dz B(z)\phi'(z) e^{-ikz} \\ &= k \sum_{k'} k' c_{k'} \frac{1}{L} \int dz B(z) e^{-i(k-k')z} \\ &= k \sum_{k'} \tilde{B}(k-k') k' c_{k'}, \end{aligned} \quad (\text{A17})$$

where

$$\tilde{B}(k-k') = \frac{1}{L} \int_{-L/2}^{L/2} dz e^{-i(k-k')z} \frac{\hbar^2}{2m^*(z)}. \quad (\text{A18})$$

In case effective mass terms are absent, $m^*(z) = m$, $\tilde{B}(k-k')$ is simply equal to $\frac{\hbar^2}{2m} \delta_{k,k'}$ and one recovers in $\tilde{h}_{k,k'}$ the usual kinetic term $\frac{\hbar^2}{2m} k^2$. Summing the \tilde{B} and \tilde{U} terms, one finds the Hamiltonian matrix

$$\tilde{h}_{k,k'} = k\tilde{B}(k-k')k' + \tilde{U}(k-k'). \quad (\text{A19})$$

APPENDIX B: DETAILS ON THE STATIC RESPONSE THEORY

Further details on the static response theory are given in what follows, and in particular the key equation (28) is derived. The starting point is the formula for the density fluctuation (24), using which χ can be expressed as the functional

derivative

$$\chi(\mathbf{x}, \mathbf{x}') = \left. \frac{\delta \rho_v(\mathbf{x})}{\delta v(\mathbf{x}')} \right|_{v=0}. \quad (\text{B1})$$

We now want to prove that the dependence of the energy on the perturbation is instead quadratic. Indeed, this can be verified by first expanding $E[v]$ (understood as a functional of v) around the unperturbed system $v = 0$, namely [30],

$$\begin{aligned} E[v] - E[0] &= \int d\mathbf{x} \left. \frac{\delta E}{\delta v(\mathbf{x})} \right|_{v=0} v(\mathbf{x}) + \frac{1}{2} \int d\mathbf{x} \int d\mathbf{x}' \\ &\times \left. \frac{\delta^2 E}{\delta v(\mathbf{x}) \delta v(\mathbf{x}')} \right|_{v=0} v(\mathbf{x})v(\mathbf{x}'). \end{aligned} \quad (\text{B2})$$

Then, we notice that $\left. \frac{\delta E}{\delta v(\mathbf{x})} \right|_{v=0} = \rho_v(\mathbf{x})$ as the external potential enters $E[v]$ the energy with the term $\int d\mathbf{x} v(\mathbf{x})\rho(\mathbf{x})$ and thus

$\left. \frac{\delta E}{\delta v(\mathbf{x})} \right|_{v=0} = \rho_0$. Differentiating the energy twice and inserting Eq. (B1), moreover, we find

$$\frac{\delta^2 E[v]}{\delta v(\mathbf{x}) \delta v(\mathbf{x}')} = \frac{\delta \rho_v(\mathbf{x})}{\delta v(\mathbf{x}')} = \chi(\mathbf{x}, \mathbf{x}'). \quad (\text{B3})$$

Therefore, Eq. (B2) can be recast as [30]

$$\begin{aligned} E[v] - E[0] &= \int d\mathbf{x} v(\mathbf{x})\rho_0 + \frac{1}{2} \int d\mathbf{x} \int d\mathbf{x}' \\ &\times \chi(\mathbf{x}, \mathbf{x}') v(\mathbf{x})v(\mathbf{x}'), \end{aligned} \quad (\text{B4})$$

and we immediately see that the first-order term vanishes, v being periodic. (A more general argument is presented in Ref. [48]). We also remind that the homogeneous matter response depends only on $\mathbf{x} - \mathbf{x}'$ due to translational invariance, i.e., $\chi(\mathbf{x}, \mathbf{x}') = \chi(\mathbf{x} - \mathbf{x}')$.

Then one can transform Eq. (B4) to momentum space inserting the Fourier expansions

$$\delta \rho(\mathbf{x}) = \sum_{\mathbf{k}} \rho_{\mathbf{k}} e^{i\mathbf{k}\cdot\mathbf{x}}, \quad v(\mathbf{x}) = \sum_{\mathbf{k}} v_{\mathbf{k}} e^{i\mathbf{k}\cdot\mathbf{x}}, \quad (\text{B5})$$

$$\chi(\mathbf{x} - \mathbf{x}') = \frac{1}{\Omega} \sum_{\mathbf{k}} \chi(\mathbf{k}) e^{i\mathbf{k}\cdot(\mathbf{x}-\mathbf{x}')}. \quad (\text{B6})$$

Then

$$E[v] - E[0] = \frac{\Omega}{2} \sum_{\mathbf{k}} v_{\mathbf{k}} \chi(\mathbf{k}) v_{-\mathbf{k}}. \quad (\text{B7})$$

If the monochromatic potential (25) is considered in place of a generic perturbation, and if the relations $\rho_0 = A/\Omega$ and $\chi = \chi(|\mathbf{q}|)$ that hold for uniform matter are employed, we find that the energy per particle of the perturbed system is given by [30]

$$\delta e_v = e_v - e_0 = \frac{\chi(q)}{\rho_0} v_q^2. \quad (\text{B8})$$

Similarly, it follows from Eq. (B5) that only the $\mathbf{k} = \pm \mathbf{q}$ components are nonvanishing and

$$\rho_q = \chi(q) v_q. \quad (\text{B9})$$

APPENDIX C: EDF RESPONSE IN THE THERMODYNAMIC LIMIT

The dynamic response of a large class of generalized Skyrme EDFs has been determined in the thermodynamic limit analytically in Ref. [24] and references therein. We summarize the main formulas here for the case of PNM and SNM. A slightly different notation is also introduced.

First, for later convenience we define K_{bulk} as

$$K_{\text{bulk}} = \sum_{\gamma} c_{\gamma} \gamma (\gamma + 1) \rho^{\gamma-1}. \quad (\text{C1})$$

Then, the following W functions are defined as in Ref. [24]:

$$W_1(q)/g = K_{\text{bulk}} - \left(2C^{\Delta\rho} + \frac{C^{\tau}}{2} \right) q^2, \quad (\text{C2})$$

$$W_2/g = C^{\tau}, \quad (\text{C3})$$

$$W_{so}/g = C^{\nabla J}. \quad (\text{C4})$$

W_2 is a constant proportional to C^{τ} , while W_1 mixes the C^{τ} and C^{δ} coefficients and carries a momentum dependence through q^2 . Lastly, W_{so} is a spin-orbit constant.

Now, we introduce adimensional functions X and insert them into $\chi(q)$ (eq. (67), Ref. [24]). With $k = q/2q_F$, we define $\tilde{\rho}$ as ρ in SNM and 2ρ in PNM. With this trick, the expressions for SNM [58] and PNM [59] are identical. The X

functions are derived from the corresponding W functions by means of

$$X_1 = \frac{m^* c^2}{(\hbar c)^2} \tilde{\rho} \frac{W_1(q)}{q_F^2}, \quad (\text{C5})$$

$$X_2 = \frac{m^* c^2}{(\hbar c)^2} \tilde{\rho} W_2, \quad (\text{C6})$$

$$X_{so} = \frac{m^* c^2}{(\hbar c)^2} \tilde{\rho} W_{so}. \quad (\text{C7})$$

We further elaborate on X_1 by splitting it as the sum of a bulk and a momentum-dependent contribution

$$X_1(k) = X_{\text{bulk}} + X_{\text{surf}}(k) \quad (\text{C8})$$

with

$$X_{\text{bulk}} = g \frac{m^* c^2}{(\hbar c)^2} \frac{\tilde{\rho}}{q_F^2} K_{\text{bulk}}, \quad (\text{C9})$$

$$X_{\text{surf}}(k) = -4g \left(2C^{\Delta\rho} + \frac{C^{\tau}}{2} \right) \frac{m^* c^2}{(\hbar c)^2} \tilde{\rho} k^2. \quad (\text{C10})$$

Finally, by using $\chi(q) = -\rho 2m_{-1}(q)/A$, with m_{-1} being the inverse energy-weighted sum rule of the strength function, and collecting some constant factors, one ends up with following formula for the TL response of a nuclear EDF:

$$\begin{aligned} \chi(q) = & -3 \frac{m^* c^2}{(\hbar c)^2} \frac{\rho}{q_F^2} f(k) \left[\left(1 + \frac{3}{8} X_2 \right)^2 + \frac{3}{4} (X_1(k) + X_2(1 - k^2)) f(k) \right. \\ & \left. - \frac{3}{64} X_2^2 \left(2 + \frac{26}{3} k^2 + (1 - k^2) f(k) \right) f(k) - \frac{3}{8} k^2 f(k) X_{so}^2 (1 + 3(1 - k^2) f(k)) \right]^{-1} \end{aligned} \quad (\text{C11})$$

with $f(k)$ defined in Eq. (33).

APPENDIX D: STATIC RESPONSE FROM DENSITY AND ENERGY FITS

The static response can be extracted either from the energies or the densities of the perturbed system. In the results presented in Sec. IV, $\chi(q)$ was obtained by energy changes. In this Appendix, we discuss fits of the density changes and show evidence that the two techniques give close outcomes.

In the linear response regime, the relation (27) holds and relates the Fourier component of the density fluctuation of the same momentum \mathbf{q} as that of the external potential. If nonlinear effects come into play, also higher-order harmonics are excited [60]. In order to extract $\chi(q)$, calculations are

performed at a given momentum q for several strengths v_q and the corresponding densities $\delta\rho(z)$ are Fourier-transformed, i.e.,

$$\rho_k = \frac{1}{L} \int dz \delta\rho(z) e^{-ikz}. \quad (\text{D1})$$

Then, the component with $k = q$ is selected. Other harmonics would be related to nonlinear contributions and do not involve the function $\chi(q)$, as discussed in Ref. [60]. Finally, a linear fit to the amplitudes ρ_q as a function of v_q is performed.

We have studied the case of PNM with $N = 66$ neutrons at a reference density $\rho_0 = 0.16 \text{ fm}^{-3}$ for the SLy4 EDF. Calculations for v_q/E_F between 0.01 and 0.1 have been performed.

TABLE II. Infinite nuclear matter coefficients L , K_0 , and K_{sym} (in MeV) and CSR $-\chi(0)/\rho$ (in MeV^{-1}) in SNM and PNM for three EDFs. The coefficients are taken from Ref. [61].

EDF	L	K_0	K_{sym}	$-\chi(0)/\rho$ (SNM)	$-\chi(0)/\rho$ (PNM)
SLy4	45.94	229.91	-119.73	0.0391	0.0233
SKM*	45.78	216.61	-155.94	0.0415	0.0268
SKI3	100.53	258.19	73.04	0.0348	0.00963

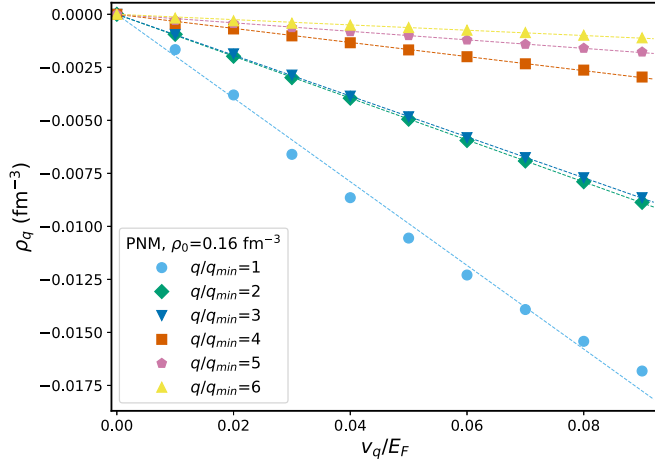


FIG. 18. Density amplitudes ρ_q as a function of the perturbation strength v_q/E_F in PNM ($N = 66$ neutrons) at a reference density $\rho_0 = 0.16 \text{ fm}^{-3}$ for the SLy4 EDF for different moments q/q_{\min} . Markers: results of the DFT calculations. Dashed lines: linear fits to the data points.

In Fig. 18 the density amplitudes ρ_q are shown as a function of the perturbation strength for different momenta as markers. Dashed lines represent linear fits to the data. A distinct linear trend of the amplitudes can be noted in all cases, with some fluctuations appearing only for $q/q_{\min} = 1$. Indeed, the response is strongest at $q/q_{\min} = 1$ (about two times stronger than for $q/q_{\min} = 2$, see Figs. 13 and 19). As a consequence, nonlinear effects are expected to play a relevant role in this case even for moderate perturbation strengths. In Fig. 18, in particular, they manifest themselves in mild deviations of the amplitudes from the linear trend. These deviations are also similar to those observed in the energies per particle for $q/q_{\min} = 1$ in the FG case (Fig. 5).

In Fig. 19 we compare the response function extracted from fits to the density (triangles) and to the energy (circles). In the inset, the relative discrepancy between the two fits, i.e.,

$$\frac{\Delta\chi}{\chi} = \frac{-\chi_{\text{Energy}} + \chi_{\text{Density}}}{(\chi_{\text{Energy}} + \chi_{\text{Density}})/2}, \quad (\text{D2})$$

is shown. It can be appreciated that it remains within a modest 5% and, with the exception of the first allowed momentum $2\pi/L$, is much smaller for the momenta below $3k_F$. We conclude that the two ways to extract the response function essentially agree.

APPENDIX E: COMPRESSIBILITY SUM RULE

The compressibility sum rule (CSR), which has been discussed in detail in Refs. [28,40], relates the static

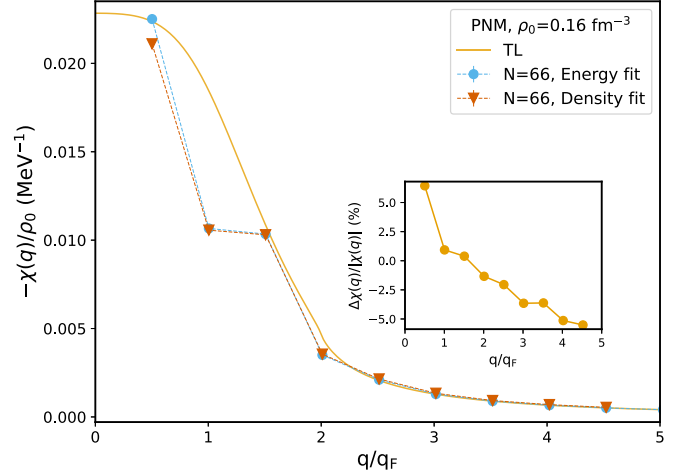


FIG. 19. Static response function $-\chi(q)/\rho_0$ extracted from fits to the energies (circles) and densities (triangles) of the perturbed system. The TL response is also shown for comparison. Inset: relative difference (in percentage) between the response function from density fits and energy fits ($\Delta\chi/|\chi|$).

response at zero momentum to the properties of unperturbed matter

$$-\frac{1}{\chi(0)} = \frac{1}{\rho} \frac{\partial P}{\partial \rho} = \frac{\partial^2 e}{\partial^2 \rho}(\rho e). \quad (\text{E1})$$

Here, we relate the CSR to the infinite matter parameters of an EDF, namely, L , K_0 , and K_{sym} (see Refs. [1,61] and below). First, we write

$$-\frac{1}{\chi(0)/\rho} = 2\rho \frac{\partial e}{\partial \rho} + \rho^2 \frac{\partial^2 e}{\partial^2 \rho}. \quad (\text{E2})$$

Then, we use $\frac{\partial e}{\partial \rho} = 0$ and $K_0 = 9\rho^2 \frac{\partial^2 e}{\partial^2 \rho}$ in SNM, and $L = 3\rho \frac{\partial e}{\partial \rho}$ and $K_{PNM} = K_0 + K_{\text{sym}} = 9\rho^2 \frac{\partial^2 e}{\partial^2 \rho}$ in PNM. Finally,

$$-\frac{1}{\chi(0)/\rho} = \frac{K_0}{9} \quad (\text{SNM}), \quad (\text{E3})$$

$$-\frac{1}{\chi(0)/\rho} = \frac{2}{3}L + \frac{K_0 + K_{\text{sym}}}{9} \quad (\text{PNM}). \quad (\text{E4})$$

In Table II we report the nuclear matter coefficients, taken from Ref. [61], and calculate the corresponding zero-momentum responses for the three representative EDFs discussed in Sec. IV C. One can note that SNM values are consistent, while in Ski3 the PNM response is smaller by a value of 2 from that of the other two EDFs. This can be traced to Ski3 having a positive K_{sym} coefficient and a slope L twice as large as that of SLy4 and SkM*.

- [1] X. Roca-Maza and N. Paar, *Prog. Part. Nucl. Phys.* **101**, 96 (2018).
 [2] M. Thiel, C. Sfienti, J. Piekarewicz, C. J. Horowitz, and M. Vanderhaeghen, *J. Phys. G: Nucl. Part. Phys.* **46**, 093003 (2019).

- [3] G. F. Burgio and I. Vidaña, *Universe* **6**, 119 (2020).
 [4] P. Haensel, A. Y. Potekhin, and D. G. Yakovlev, *Neutron Stars I: Equation of State and Structure*, Vol. 326 (Springer, New York, 2007).

- [5] G. Burgio, H.-J. Schulze, I. Vidaña, and J.-B. Wei, *Prog. Part. Nucl. Phys.* **120**, 103879 (2021).
- [6] J. Piekarewicz, The nuclear physics of neutron stars, [arXiv:2209.14877](https://arxiv.org/abs/2209.14877) [nucl-th].
- [7] A. Bulgac, M. M. Forbes, and P. Magierski, in *The BCS-BEC Crossover and the Unitary Fermi Gas*, Lecture Notes in Physics (Springer, Berlin/Heidelberg, 2011), pp. 305–373.
- [8] S. Gandolfi, A. Gezerlis, and J. Carlson, *Annu. Rev. Nucl. Part. Sci.* **65**, 303 (2015).
- [9] M. Hjorth-Jensen, M. Lombardo, and U. van Kolck, *An Advanced Course in Computational Nuclear Physics Bridging the Scales from Quarks to Neutron Stars*, Lecture Notes in Physics, Vol. 936 1st ed. (Springer International Publishing, Cham, 2017).
- [10] H. Hergert, *Front. Phys.* **8**, 379 (2020).
- [11] A. Ekström, C. Forssén, G. Hagen, G. R. Jansen, W. Jiang, and T. Papenbrock, *Front. Phys.* **11**, 1129094 (2023).
- [12] *Energy Density Functional Methods for Atomic Nuclei*, edited by N. Schunck (IOP Publishing, Bristol, 2019), pp. 2053–2563.
- [13] G. Colò, *Adv. Phys.: X* **5**, 1740061 (2020).
- [14] R. M. Martin, *Electronic Structure: Basic Theory and Practical Methods*, 2nd ed. (Cambridge University Press, Cambridge, 2020).
- [15] M. Oertel, M. Hempel, T. Klähn, and S. Typel, *Rev. Mod. Phys.* **89**, 015007 (2017).
- [16] P. Maris, J. P. Vary, S. Gandolfi, J. Carlson, and S. C. Pieper, *Phys. Rev. C* **87**, 054318 (2013).
- [17] M. M. Forbes, A. Gezerlis, K. Hebeler, T. Lesinski, and A. Schwenk, *Phys. Rev. C* **89**, 041301(R) (2014).
- [18] E. Rrapaj, A. Roggero, and J. W. Holt, *Phys. Rev. C* **93**, 065801 (2016).
- [19] S. Shen, G. Colò, and X. Roca-Maza, *Phys. Rev. C* **99**, 034322 (2019).
- [20] B. S. Pudliner, A. Smerzi, J. Carlson, V. R. Pandharipande, S. C. Pieper, and D. G. Ravenhall, *Phys. Rev. Lett.* **76**, 2416 (1996).
- [21] S. Gandolfi, J. Carlson, and S. C. Pieper, *Phys. Rev. Lett.* **106**, 012501 (2011).
- [22] A. Boulet and D. Lacroix, *Phys. Rev. C* **97**, 014301 (2018).
- [23] L. Riz, S. Gandolfi, and F. Pederiva, *J. Phys. G: Nucl. Part. Phys.* **47**, 045106 (2020).
- [24] A. Pastore, D. Davesne, and J. Navarro, *Phys. Rep.* **563**, 1 (2015).
- [25] D. Davesne, A. Pastore, and J. Navarro, *Prog. Part. Nucl. Phys.* **120**, 103870 (2021).
- [26] M. Buraczynski and A. Gezerlis, *Phys. Rev. Lett.* **116**, 152501 (2016).
- [27] M. Buraczynski and A. Gezerlis, *Phys. Rev. C* **95**, 044309 (2017).
- [28] M. Buraczynski, S. Martinello, and A. Gezerlis, *Phys. Lett. B* **818**, 136347 (2021).
- [29] S. Moroni, D. M. Ceperley, and G. Senatore, *Phys. Rev. Lett.* **75**, 689 (1995).
- [30] G. Senatore, S. Moroni, and D. M. Ceperley, in *Quantum Monte Carlo Methods in Physics and Chemistry*, edited by M. Nightingale and C. J. Umrigar (Springer, Netherlands, 1999).
- [31] T. Dornheim, S. Groth, J. Vorberger, and M. Bonitz, *Phys. Rev. E* **96**, 023203 (2017).
- [32] J. Carlson and S. Gandolfi, *Phys. Rev. A* **90**, 011601(R) (2014).
- [33] J. Carlson, S. Gandolfi, F. Pederiva, S. Pieper, R. Schiavilla, K. E. Schmidt, and R. B. Wiringa, *Rev. Mod. Phys.* **87**, 1067 (2015).
- [34] I. Tews, *Front. Phys.* **8**, 153 (2020).
- [35] J. G. Lietz, S. Novario, G. R. Jansen, G. Hagen, and M. Hjorth-Jensen, *An Advanced Course in Computational Nuclear Physics*, Lecture Notes in Physics Vol. 936 (Springer International Publishing, Cham, 2017), pp. 293–399.
- [36] G. Hagen, T. Papenbrock, A. Ekström, K. A. Wendt, G. Baardsen, S. Gandolfi, M. Hjorth-Jensen, and C. J. Horowitz, *Phys. Rev. C* **89**, 014319 (2014).
- [37] C. Barbieri and A. Carbone, Self-consistent Green’s Function Approaches, in *An Advanced Course in Computational Nuclear Physics: Bridging the Scales from Quarks to Neutron Stars*, edited by M. Hjorth-Jensen, M. P. Lombardo, and U. van Kolck (Springer International Publishing, Cham, 2017), pp. 571–644.
- [38] P. Arthuis, C. Barbieri, F. Pederiva, and A. Roggero, *Phys. Rev. C* **107**, 044303 (2023).
- [39] M. Piarulli, I. Bombaci, D. Logoteta, A. Lovato, and R. B. Wiringa, *Phys. Rev. C* **101**, 045801 (2020).
- [40] M. Buraczynski, S. Martinello, and A. Gezerlis, *Phys. Rev. C* **105**, 025807 (2022).
- [41] F. Marino, C. Barbieri, A. Carbone, G. Colò, A. Lovato, F. Pederiva, X. Roca-Maza, and E. Vigezzi, *Phys. Rev. C* **104**, 024315 (2021).
- [42] F. Dalfovo, A. Lastrì, L. Pricauptenko, S. Stringari, and J. Treiner, *Phys. Rev. B* **52**, 1193 (1995).
- [43] A. L. Fetter and J. D. Walecka, *Quantum Theory of Many-Particle Systems* (McGraw-Hill, Boston, 1971).
- [44] A. Rios, *Front. Phys.* **8**, 387 (2020).
- [45] P. Danielewicz and J. Lee, *Nucl. Phys. A* **818**, 36 (2009).
- [46] J. Izaac, *Computational Quantum Mechanics*, 1st ed., Undergraduate Lecture Notes in Physics (Springer International Publishing, Cham, 2018).
- [47] G. Colò, L. Cao, N. V. Giai, and L. Capelli, *Comput. Phys. Commun.* **184**, 142 (2013).
- [48] G. Giuliani and G. Vignale, *Quantum Theory of the Electron Liquid* (Cambridge University Press, Cambridge, 2005).
- [49] *Theory of the Inhomogeneous Electron Gas*, edited by S. Lundqvist and N. H. March (Springer, Boston, 1983).
- [50] S. Groth, T. Dornheim, and M. Bonitz, *J. Chem. Phys.* **147**, 164108 (2017).
- [51] R. N. Bisset, P. B. Blakie, and S. Stringari, *Phys. Rev. A* **100**, 013620 (2019).
- [52] B. Mihaila, Lindhard function of a d-dimensional Fermi gas, [arXiv:1111.5337](https://arxiv.org/abs/1111.5337) [cond-mat.quant-gas] (2011).
- [53] E. Chabanat, P. Bonche, P. Haensel, J. Meyer, and R. Schaeffer, *Nucl. Phys. A* **627**, 710 (1997).
- [54] J. Lynn, I. Tews, S. Gandolfi, and A. Lovato, *Annu. Rev. Nucl. Part. Sci.* **69**, 279 (2019).
- [55] J. Bartel, P. Quentin, M. Brack, C. Guet, and H.-B. Håkansson, *Nucl. Phys. A* **386**, 79 (1982).
- [56] P.-G. Reinhard and H. Flocard, *Nucl. Phys. A* **584**, 467 (1995).
- [57] F. Marino, G. Colò, A. Lovato, F. Pederiva, X. Roca-Maza, and E. Vigezzi (unpublished).
- [58] A. Pastore, D. Davesne, Y. Lallouet, M. Martini, K. Bennaceur, and J. Meyer, *Phys. Rev. C* **85**, 054317 (2012).
- [59] A. Pastore, M. Martini, V. Buridon, D. Davesne, K. Bennaceur, and J. Meyer, *Phys. Rev. C* **86**, 044308 (2012).
- [60] T. Dornheim, M. Böhme, Z. A. Moldabekov, J. Vorberger, and M. Bonitz, *Phys. Rev. Res.* **3**, 033231 (2021).
- [61] M. Dutra, O. Lourenço, J. S. Sá Martins, A. Delfino, J. R. Stone, and P. D. Stevenson, *Phys. Rev. C* **85**, 035201 (2012).